Journal of Applied Electrochemistry **32**: 35–41, 2002.

The study of aluminium corrosion in acidic solution with nontoxic inhibitors

M. METIKOŠ-HUKOVIĆ[1]*, R. BABIĆ[2] and Z. GRUBAČ[2]
[1]*Department of Electrochemistry, Faculty of Chemical Engineering and Technology, University of Zagreb, 10000 Zagreb, PO Box 177, Croatia*
[2]*Department of General and Inorganic Chemistry, Faculty of Chemical Technology, University of Split, Auquery 21000 Split, N. Tesle 10, Croatia*
*(*author for correspondence, fax: +(385 1) 4597 139, e-mail: mmetik@marie.fkit.hr)*

Received 13 March 2001; accepted in revised form 11 September 2001

Key words: aluminium, corrosion inhibition, impedance spectroscopy, *N*-arylpyrroles

Abstract

The inhibitory activity of some substituted *N*-arylpyrroles on aluminium corrosion in hydrochloric acid was studied in relation to inhibitor concentration, using potentiodynamic and impedance spectroscopy techniques. All investigated compounds were found to act as cathodic-type inhibitors and inhibition was ascribed to the adsorption of inhibitor onto the electrode surface. The inhibiting efficiency of the additives depended on the inductive power of the groups attached to the benzene and/or pyrrole ring. The carbaldehyde group showed better inhibiting power due to additional condensation on the electrode surface. The impedance results analysed in terms of the polarization resistance showed that the EIS technique can be successfully applied in the determination of corrosion resistance in systems where the corrosion kinetics are not simple.

List of symbols

B Stern–Geary constant
b Tafel slope (V decade^{-1})
c concentration (M)
E potential (V)
f frequency (Hz)
j current density (A cm^{-2})
jω complex variable for sinusoidal perturbations with $\omega = 2\pi$f
L inductance (H cm^2)
n characteristic parameter of constant phase element (CPE)
Q coefficient reflecting combination of properties related to surface and electroactive species (Ω^{-1} cm^{-2} s^n)
R resistance (Ω cm^2)
Z impedance (Ω cm^2)

Greek letters
η inhibiting efficiency
v sweep rate (V s^{-1})
ω angular speed (rad s^{-1})

Sub- and superscripts
c cathodic
corr corrosion
el electrolyte
i inhibitor
p polarization
tot total

1. Introduction

Although aluminium is a reactive metal ($E^\circ = -1.66$ V vs SHE), it is resistant to corrosion in solutions of pH between 4 and 9, whenever aggressive ions, such as chloride, are not present [1]. This resistance is attributed to the presence of a thin, adherent and protective surface oxide film. Above and below this pH range, solubility of the oxide film increases, and aluminium exhibits uniform attack [1].

Hydrochloric acid solution is used for electrochemical etching of aluminium foil and lithographic plates. Because HCl is an aggressive medium, inhibitors are often used to reduce the corrosion of metals. A number of organic compounds have been described as aluminium corrosion inhibitors in hydrochloric acid solution [2–14], the majority being nitrogen-containing compounds [2, 5–14]. Many *N*-heterocyclic compounds with polar groups and/or π-electrons are efficient corrosion inhibitors in acidic solutions. Organic molecules of this type can absorb on the metal surface and form a bond between the *N* electron pair and/or the π-electron cloud and the metal, thereby reducing the corrosion in acidic solution [2, 15].

It was shown, in a previous study, that substituted *N*-arylpyrroles acted as cathodic-type corrosion inhibitors of aluminium in perchloric acid solution [16], and iron in hydrochloric acid solution [17, 18]. Inhibiting properties of 1-(2-chlorophenyl)–2,5-dimethylpyrrole–3,4-dicarbaldehyde on aluminium in hydrochloric acid solution were also studied [9]. It was found that the position and number of functional groups in the pyrrol, or the benzene ring, strongly influence the inhibiting efficiency.

The aim of the present work was to study the inhibiting properties of six substituted *N*-arylpyrroles on the corrosion of aluminium in 0.5 M hydrochloric acid solution. The investigation was performed using potentiodynamic and electrochemical impedance spectroscopy (EIS) measurements.

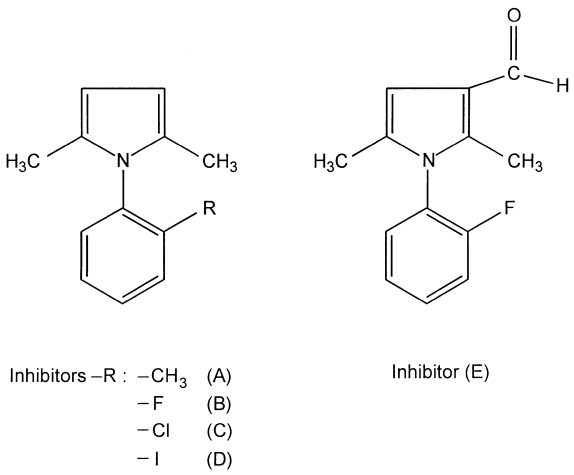

Fig. 1. Chemical structure of the investigated compounds.

2. Experimental details

The sample selected for the study was 99.6% pure aluminium. Disc electrodes were machined from a cylindrical rod 8 mm in diameter, and moulded in polyester. Prior to each electrochemical experiment, the electrode surface was abraded with emery paper to an 800 metalographic finish, exposed to a hot (40 °C) 1.0 mol dm^{-3} sodium hydroxide solution for 15 s, rinsed with distilled water, left for 10 min in the atmosphere and immersed in the electrolyte solution for 10 min. This procedure gave good reproducibility of results. In all measurements, the counter electrode was a platinum gauze and the reference electrode was a saturated calomel electrode (SCE). All potentials are referred to the SCE.

The measurements were performed in 0.5 mol dm^{-3} hydrochloric solution deaerated with nitrogen without and with the presence of six substituted *N*-arylpyrroles in the concentration range from 5×10^{-5} to 5×10^{-3} M. Substituted *N*-arylpyrroles were:

(A) 1-(2-methylphenyl)–2,5-dimethylpyrrole
(B) 1-(2-fluorophenyl)–2,5-dimethylpyrrole
(C) 1-(2-chlorophenyl)–2,5-dimethylpyrrole
(D) 1-(2-iodophenyl)–2,5-dimethylpyrrole
(E) 1-(2-fluorophenyl)–2,5-dimethylpyrrole–3-carbaldehyde.

The structural formulae of the investigated compounds are presented in Figure 1. The compounds were synthesized by Knorr–Paal condensation of 2,5-hexadione with the corresponding anilines [19].

The measurements were carried out in a standard electrochemical cell with a separate compartment for the reference electrode connected to the main compartment via a Luggin capillary. The cell was a water-jacket version, connected to a constant temperature circulator.

The polarization curves, E against j, were obtained using the linear potential sweep technique at a sweep rate of 10 mV s^{-1}, going from the corrosion potential to the cathodic and then to the anodic side. The polarization resistances, R_p were determined from the slope of the polarization curves in the potential range from −20 mV to +10 mV from the corrosion potential. This measurement was performed with a sweep rate of 0.1 mV s^{-1}.

Impedance measurements were performed in the frequency range from 60 kHz to 50 mHz with an a.c. amplitude ±5 mV. All measurements were performed using a PAR potentiostat model 273A and a PAR lock-in amplifier model 5301A controlled by a personal computer.

3. Results and discussion

3.1. *Polarization behaviour*

Examples of potentiodynamic polarization curves for Al in hydrochloric acid solution, containing various substituted *N*-arylpyrroles, are shown in Figures 2 and 3. In all cases, addition of inhibitors induced a negligible decrease in the anodic currents, and a significant decrease in the cathodic currents. The observed decrease in cathodic current was the greatest for 1-(2-fluorophenyl)–2,5-dimethylpyrrole–3-carbaldehyde (inhibitor E)

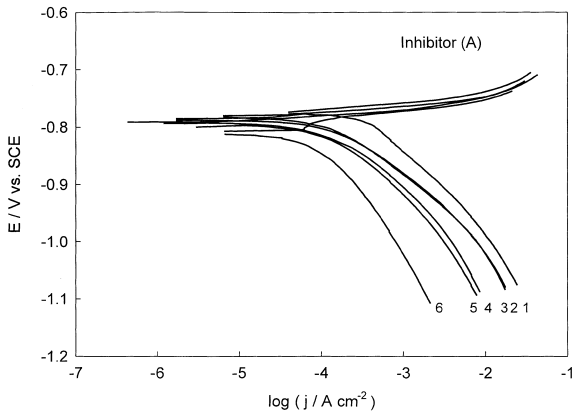

Fig. 2. Tafel plots for aluminium in 0.5 M hydrochloric acid solution without and in the presence of different concentration (c) of 1-(2-methylphenyl)–2,5-dimethylpyrrole, (inhibitor A). Key for c: (1) 0, (2) 5×10^{-5}, (3) 1×10^{-4}, (4) 5×10^{-4}, (5) 1×10^{-3} and (6) 5×10^{-3} M.

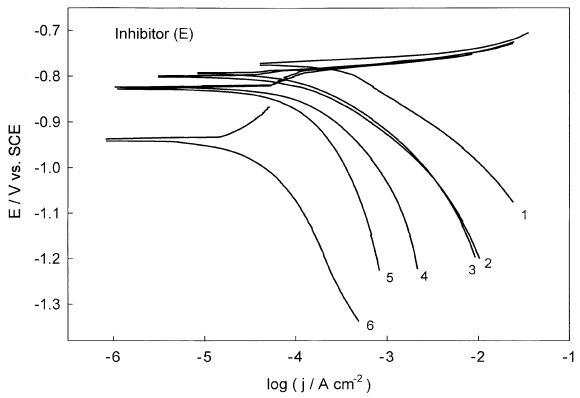

Fig. 3. Tafel plots for aluminium in 0.5 M hydrochloric acid solution without and in the presence of different concentration (c) of 1-(2-fluorophenyl)–2,5-dimethylpyrrole–3-carbaldehyde, (inhibitor E). Key for c: (1) 0, (2) 5×10^{-5}, (3) 1×10^{-4}, (4) 5×10^{-4}, (5) 1×10^{-3} and (6) 5×10^{-3} M.

(Figure 3), somewhat less for 1-(2-fluorophenyl)–2,5-dimethylpyrrole (inhibitor B), and almost the same for all other inhibitors (Figure 2). The value of E_{corr} was not affected by the addition of inhibitors except for inhibitor E, an increase in its concentration shifted the corrosion potential in the negative direction. None of the inhibitors affected the anodic Tafel slope, which was around 58 mV. The cathodic Tafel slope of approximately 224 mV was observed in purely acidic solution, in the presence of all inhibitors (Table 1) except for inhibitor E. By increasing its concentration from zero to 5×10^{-3} M, the cathodic Tafel slope b_c gradually changed from 224 to 348 mV (Table 2). The cathodic Tafel slopes, b_c, above 180 mV indicate that the hydrogen evolution reaction takes place at the metal covered by a surface layer, probably an oxide or an oxide-inhibitor complex, which acts as a potential energy barrier to the charge carriers [20, 21].

Taking into account all polarization characteristics it can be concluded that, because they significantly affect the cathodic polarization process, all investigated substituted *N*-arylpyrroles, can be classified as cathodic-type inhibitors. However, cathodic Tafel slopes for inhibitors A to D were approximately constant, which suggests that the inhibiting action occurred by simple blocking of the available cathodic sites on the metal surface, which led to a decrease in the exposed area necessary for hydrogen evolution and lowered the dissolution rate with increasing inhibitor concentration. The shift of E_{corr} towards more negative values, as observed in the presence of inhibitor E, indicates that this compound prevents localised attack on aluminium surface. Thus, the E_{corr} shift appears to be a suitable parameter for rating resistance to localized corrosion [22].

Table 1. Corrosion parameters for aluminium in 0.5 M HCl solution without and with the presence of 1-(2-methylphenyl)–2,5-dimethylpyrrole (inhibitor A)

c (inhibitor) /mol dm^{-3}	$-b_c$ /mV	$-E_{corr}$ /mV	R_p /Ω cm^2	η_{Rp} /%
0	224	792	50	–
5×10^{-5}	202	815	169	70.4
1×10^{-4}	207	803	174	71.3
5×10^{-4}	200	817	179	72.1
1×10^{-3}	206	818	219	77.2
5×10^{-3}	238	825	274	81.8

Table 2. Corrosion parameters for aluminium in 0.5 M HCl solution without and with the presence of 1-(2-fluorophenyl)–2,5-dimethylpyrrole–3-carbaldehyde (inhibitor E)

c (inhibitor) /mol dm^{-3}	$-b_c$ /mV	$-E_{corr}$ /mV	R_p /Ω cm^2	η_{Rp} /%
0	224	792	50	–
5×10^{-5}	246	800	258	80.6
1×10^{-4}	303	802	270	81.5
5×10^{-4}	325	820	289	82.7
1×10^{-3}	260	821	347	85.6
5×10^{-3}	348	891	1239	96.0

Polarization resistances, R_p for aluminium in hydrochloric acid solution, alone and in the presence of inhibitors, were determined from the current–potential curves in the vicinity of E_{corr}. Straight lines were obtained in the potential range E_{corr} −20 mV and E_{corr} +10 mV. Generally, R_p values increased with increasing inhibitor concentration, and were greatest for 1-(2-fluorophenyl)–2,5-dimethylpyrrole–3-carbaldehyde (inhibitor E), somewhat less for 1-(2-fluorophenyl)–2,5-dimethylpyrrole (inhibitor B), and almost the same for all other inhibitors. R_p values were used to calculate the inhibiting efficiency, η_{Rp} using the equation $\eta_{Rp} = (1 - R_{p,0}/R_{p,i})$, where $R_{p,0}$ is the polarization resistance for aluminium in hydrochloric acid without inhibitors, and $R_{p,i}$ is the polarization resistance in the presence of inhibitors. Tables 1 and 2 contain the values of cathodic Tafel slope, b_c, corrosion potential, E_{corr}, polarization resistance, R_p, and inhibiting efficiency, η_{Rp} for 1-(2-methylphenyl)–2,5-dimethylpyrrole and 1-(2-fluorophenyl)–2,5-dimethylpyrrole–3-carbaldehyde, respectively, at all concentrations. The values for R_p and η_{Rp} obtained for all inhibitors at $c = 5 \times 10^{-3}$ M are presented in Table 3 for comparison.

3.2. *Electrochemical impedance spectroscopy measurements*

Impedance spectra for aluminium in 0.5 M hydrochloric acid, without and in the presence of different concentrations of inhibitors, were similar in shape. The

Table 3. Polarization resistance and inhibition efficiencies for aluminium in 0.5 M HCl solution in the presence of various inhibitors at a concentration of 5×10^{-3} M

Inhibitor	R_p/Ω cm^2	η_{Rp}/%
A	274	81.8
B	285	82.5
C	182	72.5
D	264	81.1
E	1239	96.0

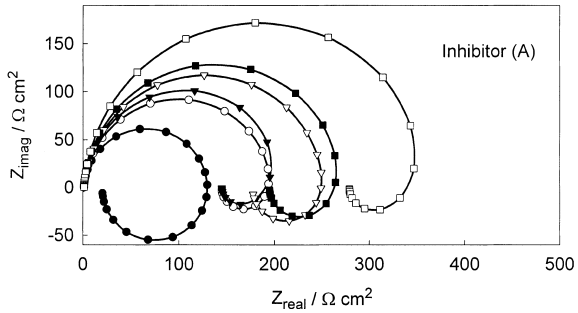

Fig. 4. Nyquist plots for aluminium in 0.5 M hydrochloric acid solution without (●) and in the presence of: (○) 5×10^{-5}, (▼) 1×10^{-4}, (▽) 5×10^{-4}, (■) 1×10^{-3} and (□) 5×10^{-3} M 1-(2-methylphenyl)–2,5-dimethylpyrrole, (inhibitor A).

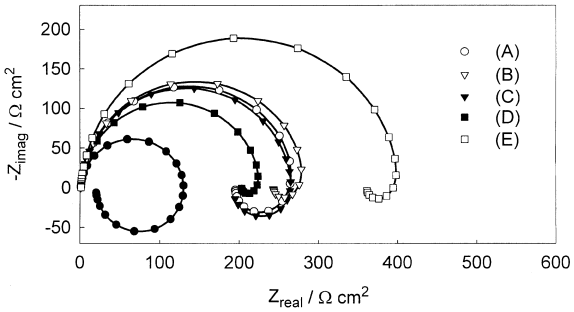

Fig. 6. Nyquist plots for aluminium in 0.5 M hydrochloric acid solution without and in the presence of all inhibitors at concentration of 1×10^{-3} M.

appearance of two semicircles in the impedance diagram was common to all systems. The high frequency semicircle corresponds to a capacitive loop and the low frequency semicircle corresponds to an inductive loop. The semicircle radii were dependent on the inhibitor used and its concentration. Nyquist plots for aluminium in hydrochloric acid, alone and in the presence of 1-(2-methylphenyl)–2,5-dimethylpyrrole (inhibitor A) and 1-(2-fluorophenyl)–2,5-dimethylpyrrole–3-carbaldehyde (inhibitor E), are presented in Figures 4 and 5, respectively. Impedance spectra, obtained in the presence of all inhibitors at $c = 5 \times 10^{-3}$ M, are presented in Figure 6 for comparison. The diameter of the high frequency capacitive semicircle markedly increased with increasing inhibitor concentration, especially in the presence of 1-(2-fluorophenyl)–2,5-dimethylpyrrole–3-carbaldehyde (inhibitor E), indicating its superior inhibiting properties.

Figures show that at least two time constants can be observed in all cases. The first time constant corresponds to the capacitive loop at higher frequencies and the second to the inductive loop at lower frequencies (up to 50 mHz). In the investigated frequency range, similar impedance plots were reported for aluminium in various electrolytes such as hydrochloric acid [9, 23–25], sulfuric acid [26, 27], sodium chloride [28, 29], sodium sulfate [26, 29] and acetic acid [27]. In some of the mentioned cases, a third time constant (a capacitive loop) was also observed, but only in the frequency range from about 100 to 1 mHz.

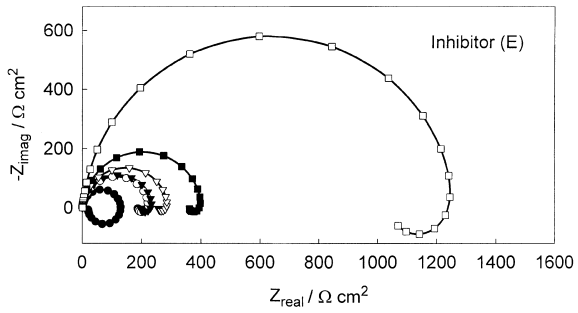

Fig. 5. Nyquist plots for aluminium in 0.5 M hydrochloric acid solution without (●) and in the presence of: (○) 5×10^{-5}, (▼) 1×10^{-4}, (▽) 5×10^{-4}, (■) 1×10^{-3} and (□) 5×10^{-3} M 1-(2-fluorophenyl)–2,5-dimethylpyrrole–3-carbaldehyde, (inhibitor E).

As far as the origin of the different time constants is concerned, it can be concluded that there is no agreement about it. The time constant at high frequencies has often been attributed to the formation of an oxide layer or to an oxide layer itself. Brett [24, 25] attributed this time constant to the interfacial reactions, in particular to the reaction of aluminium oxidation at the metal|oxide|electrolyte interface. The process includes formation of Al^+ ions at the metal|oxide interface, and their migration through the oxide layer due to a high electric field strength, to the oxide|solution interface where they become oxidized to Al^{3+}. At the oxide|solution interface, OH^- or O^{2-} ions are also formed. The fact that all these processes are represented by only one time constant could be understood either by overlapping of the time constants of separate processes, or by the assumption that one process dominates and, therefore, excludes the other processes [27]. The other possible explanation for the high frequency capacitive constant is the oxide film itself. This assumption was supported by a linear relationship between the inverse of the capacitance and the potential found by Bessone et al. [30] and Wit et al. [31]. The oxide film thickness observed by Lenderink et al. [27] and by Frers et al. [28], although much thinner than the naturally formed one, supported this assumption.

The origin of the inductive loop on aluminium is also not clear. It is often attributed to surface or bulk relaxation of species in the oxide layer [28]. Burstein's measurements [32, 33] confirmed that the inductive loop is closely related to the existence of a passive film on aluminium. Bessone et al. [30] suggested that the inductive time constant is the result of a rearrangement of surface charge at the metal|oxide interface. It was also proposed that adsorbed intermediates in reduction of hydrogen ions could cause an inductive loop [9, 27]. Bessone et al. [29] have observed an inductive loop for the pitted active state on aluminium and attributed it to surface area modulation or salt film property modulation. Keddam et al. [34] have proposed the same hypothesis for the anodic dissolution of aluminium in acidic sodium chloride solution. In our previous

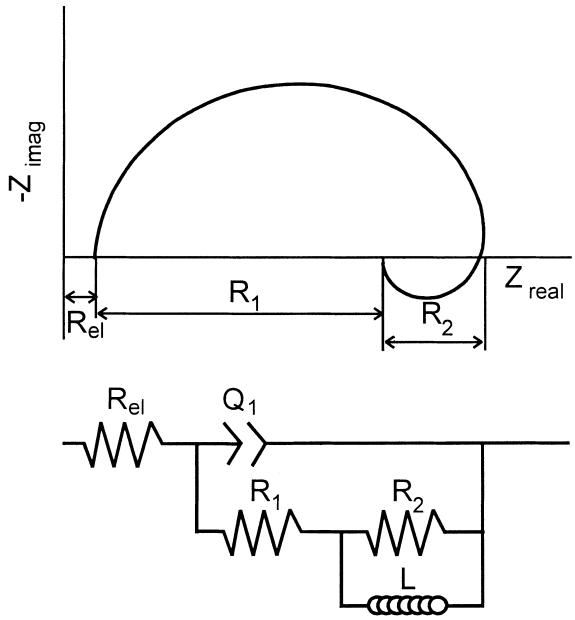

Fig. 7. Equivalent circuit diagram for total impedance (a), and complex impedance diagram for equivalent circuit (b).

investigation [9, 10] of corrosion and inhibition of aluminium in dilute hydrochloric acid solution, we correlated the high frequency capacitive loop with the properties of the oxide film itself, while the low frequency inductive loop was attributed to the slow relaxation process of hydrogen adsorption, as well as aluminium dissolution.

The equivalent circuit used to fit the experimental data is shown in Figure 7 under (a), together with its complex impedance diagram under (b). It consists of a constant phase element (CPE) Q in parallel with series resistors R_1 and R_2, and an inductance, of magnitude L, in parallel with R_2. Accordingly, the total impedance Z_{tot} is equal to the sum of R_{el} and Z_1, where Z_1 is

$$Z_1 = \left(\frac{1}{Z_{\text{CPE}}} + \frac{1}{Z_2 + R_1}\right)^{-1} \tag{1}$$

and Z_2 is

$$Z_2 = \left(\frac{1}{R_2} + \frac{1}{\mathrm{j}\omega L}\right)^{-1} \tag{2}$$

$$Z_2 = \frac{R_2^2 L(\mathrm{j}\omega) + R_2 L^2 \omega^2}{R_2^2 + \omega^2 L^2} \tag{3}$$

Thus, the total impedance is given by

$$Z_{\text{total}} = R_{\text{el}} + \left\{ Q(\mathrm{j}\omega)^n + \left(\frac{R_2^2 L(\mathrm{j}\omega) + R_2 L^2 \omega^2}{R_2^2 + \omega^2 L^2} + R_1\right)^{-1} \right\}^{-1} \tag{4}$$

The use of CPE type impedance has been extensively described in the literature for this type of study. Exponent n in Equation 5 for CPE impedance

$$Z_{\text{CPE}} = [Q(\mathrm{j}\omega)^n]^{-1} \tag{5}$$

provides information about the degree of non-ideality in capacitive behaviour. Its value makes it possible to differentiate between the behaviour of a CPE ($n < 1$) and that of an ideal capacitor ($n = 1$). In the complex impedance plot (Figure 7(b)), the value of R_1 represents the intersection point of the low-frequency semicircle on the real axis, for $\omega \to 0$. In general, the value of this intersection may be used to obtain the apparent a.c. polarization resistance R_{p}

$$R_{\text{p}} = \lim_{\omega \to 0} [Z_{\text{real}}] \tag{6}$$

The polarization resistance, R_{p} is correlated unequivocally to the corrosion current density ($j_{\text{corr}} = \text{B}/R_{\text{p}}$) in relatively simple corrosion systems characterized only by a charge transfer-controlled process. In more complicated systems, that is, in real three-dimensional inhomogeneous systems [35], because of the time-dependent formation of the porous or compact barrier layer, R_{p} is in general a complicated function determined by the rates of charge transfer, mass transport and chemical reaction [36].

For each set of experimental data, the parameters Q_1, n, R_1, R_2 and L were evaluated using a simple least square fitting procedure. The experimental data were found to be sufficiently well fitted by the transfer function of the equivalent circuit presented in Figure 7 within the limits of experimental error and reproducibility of the data.

Table 4 contains the values of impedance parameters for all inhibitors, at $c = 5 \times 10^{-3}$ M. The value of electrolyte resistance, R_{el} was around 1 Ω in all experiments.

Results show that the value of polarization resistance, R_1, increases with increasing inhibitor concentration. Since R_{p} is inversely proportional to the corrosion current, it can be used to calculate the inhibitor efficiency, $\eta_{\text{a.c.}}$:

$$\eta_{\text{a.c.}} = (R_{\text{p,i}} - R_{\text{p,0}})/R_{\text{p,i}} \tag{7}$$

where $R_{\text{p,i}}$ and $R_{\text{p,0}}$ are polarization resistances, with and without inhibitor, respectively. Inhibitor efficiency increased with increasing inhibitor concentration. The highest inhibitor efficiency was always observed in the

Table 4. Impedance parameters for aluminium in 0.5 M HCl solution in the presence of various inhibitors at a concentration of 5×10^{-3} M

Inhibitor	$10^5 \times Q_1$ /Ω^{-1} cm^{-2} s^n	n	R_1 /Ω cm^2	R_2 /Ω cm^2	L /H cm^2	$\eta_{\text{a.c.}}$ /%
A	2.81	0.96	278	91	8	93.2
B	2.43	0.96	280	82	10	93.2
C	3.06	0.96	195	80	9	90.3
D	2.42	0.96	210	24	7	91.0
E	2.11	0.94	1045	224	242	98.2

presence of 1-(2-fluorophenyl)–2,5-dimethylpyrrole–3-carbaldehyde (inhibitor E), somewhat lower in the presence of 1-(2-fluorophenyl)–2,5-dimethylpyrrole (inhibitor B) and almost equal in the presence of the other investigated *N*-arylpyrroles. The inhibitor efficiency for all inhibitors at a concentration of 5×10^{-3} M is presented in Table 4.

A comparison of the inhibiting efficiencies obtained using a.c. and d.c. methods shows that acceptable agreement is achieved. The efficiency values obtained from impedance measurements were somewhat (up to 10%) higher than those observed using the polarization technique. However, the order of magnitude was the same for both methods.

Substituted *N*-arylpyrroles A to D differ only by the substituent in the benzene ring at position 2, either the methyl, fluoro, chloro or iodo group. All, except the fluorinated *N*-arylpyrrole, showed almost equal inhibiting efficiency over the entire concentration range. 1-(2-fluorophenyl)–2,5-dimethylpyrrole showed somewhat higher (up to 5%) inhibiting efficiency by both d.c. and a.c. methods. Superior protective properties of this compound were also found by Metikos–Huković et al. [18] in investigations of iron corrosion in hydrochloric acid solution. By inserting flourine, the most electronegative element, in the *ortho* position of the benzene ring, the electron charge density of the molecule increased, leading to an accelerated and stronger adsorption on the positively charged metal surface. In the case of iron corrosion, it was shown [18] that fluorine substitution in the *ortho* position is much more effective than substitution in the *meta* and *para* positions.

The best inhibiting efficiency for aluminium corrosion in hydrochloric acid solution was observed in the presence of 1-(2-fluorophenyl)–2,5-dimethylpyrrole–3-carbaldehyde. Carbaldehyde substituted *N*-arylpyrroles also exhibited the best inhibiting efficiency for aluminium corrosion in perchloric acid [16]. Inserting the carbaldehyde group additionally increased the electron density of the inhibitor molecule, thus causing stronger adsorption on the metal surface. It was also found that insertion of the carbaldehyde group into the pyrrole ring of substituted *N*-aryl-2,5-dimethylpyrroles caused a condensation reaction between methyl and aldehyde groups, which lead to the formation of two C=C double bonds connecting two pyrrole molecules, as shown in Figure 8. A further increase in electron density, due to double bond formation, gave rise to increasing protection efficiency as a result of π-electron interaction between the inhibitor molecules and the metal.

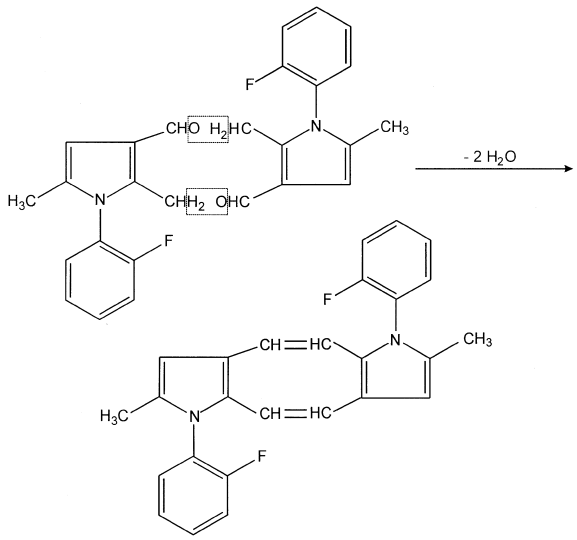

Fig. 8. Condensation product of 1-(2-fluorophenyl)–2,5-dimethylpyrrole–3-carbaldehyde, (inhibitor E).

4. Conclusions

The corrosion behaviour of aluminium was investigated in 0.5 M hydrochloric acid with and without addition of different substituted *N*-arylpyrroles, using potentiodynamic and EIS techniques.

Polarization measurements showed that all substituted *N*-arylpyrroles induced a decrease in the cathodic currents without affecting the anodic polarization behaviour. A shift of corrosion potential to the negative side was observed only in the presence of the carbaldehyde group in a pyrrole ring. The large cathodic Tafel slopes obtained in the presence of all inhibitors indicated that hydrogen evolution occurred at the metal surface covered by an oxide film-inhibitor complex, which acted as a potential-energy barrier to the charge carriers.

Impedance measurements at E_{corr} showed a high frequency capacitive loop related to the dielectric properties of the surface film and a low frequency inductive part attributed to the relaxation of adsorbed species and metal dissolution. Electrical parameters of the proposed equivalent circuit were calculated, and inhibitory efficiencies were determined.

Both polarization and impedance measurements showed that inhibitory efficiency increased with increasing inhibitor concentration. The ability of *N*-arylpyrroles to inhibit hydrogen evolution was attributed to the adsorption of inhibitor molecules, that could be modified by insertion of different functional groups with varying inductive power. The high inhibition efficiency of 1-(2-fluorophenyl)–2,5-dimethylpyrrole–3-carbaldehyde was attributed to the condensation reaction of inhibitor molecules at the electrode surface.

References

1. M. Pourbaix, *in* 'Atlas of Electrochemical Equilibria in Aqueous Solutions' (Pergamon Press, New York, 1966).
2. G. Schmitt, *Br. Corros. J.* **19** (1984) 165.
3. T. Zhao and G. Mu, *Corros. Sci.* **41** (1999) 1937.
4. R.L. Cook, Jr and S.R. Taylor, *Corrosion* **56** (2000) 321.
5. E. Khamis and M. Atea, *Corrosion* **50** (1994) 106.
6. L. Garrigues, N. Pebere and F. Dabosi, *Electrochim. Acta* **41** (1996) 1209.

7. S.S. Mahmoud and G.A. El-Mahdy, *Corrosion* **53** (1997) 437.
8. A.S. Fouda, M.N. Moussa, F.I. Taha and A.I. El Neanea, *Corros. Sci.* **26** (1986) 719.
9. M. Metikoš-Huković, R. Babić and Z. Grubač, *J. Appl. Electrochem.* **28** (1998) 433.
10. R. Babić, M. Metikoš-Huković, S. Omanović, Z. Grubač and S. Brinić, *Br. Corros. J.* **30** (1995) 288.
11. M. Metikoš-Huković, R. Babić, Z. Grubač and S. Brinić, *J. Appl. Electrochem.* **24** (1994) 325.
12. M. Metikoš-Huković, R. Babić, Z. Grubač and S. Brinić, *J. Appl. Electrochem.* **24** (1994) 772.
13. E. Khamis, B.A. Abd El-Nabey, M. Shaban, A. El-Sharnoby and G.E. Thomson, *in* Proceedings of the 7th European Symposium on 'Corrosion Inhibitors', Ann. Univ. Ferrara, N.S., Sez. V, Suppl. N. **9** (1990), p. 1173.
14. M.S. Abdel-Aal, M.Th. Makhlof and A.A. Hermas, *in* Proceedings *op. cit.* [13], N.S., Sez. V, Suppl. N. **9** (1990), p. 1143.
15. G. Trabanelli, *in* F. Mansfield (Ed.), 'Corrosion Mechanisms', (Marcel Dekker, New York, 1987), chapter 3.
16. M. Metikoš-Huković, Z. Grubać and E. Stupnišek-Lisac, *Corrosion* **50** (1994) 146.
17. E. Stupnišek-Lisac and M. Metikoš-Huković, *Br. Corros. J.* **28** (1993) 74.
18. E. Stupnišek-Lisac, M. Metikoš-Huković, D. Lenčié, J. Vorkapić-Furač and K. Berković, *Corrosion* **48** (1992) 924.
19. J. Vorkapić-Furač, M. Mintas, T. Burgemeister and A. Mannschreck, *J. Chem. Soc. Perkin Trans.* **2** (1989) 713.
20. A.K. Vijh, *J. Phys. Chem.* **73** (1969) 506.
21. R.E. Mayer, *J. Electrochem. Soc.* **113** (1966) 1158.
22. C. Monticelli, G. Brunoro and G. Trabanelli, *in* Proceedings op. cit. [13], N.S., Sez. V, Suppl. N. 9 (1990), p. 1125.
23. E.J. Lee and S.I. Pyun, *Corros. Sci.* **37** (1995) 157.
24. C.M.A. Brett, *Corros. Sci.* **33** (1992) 203.
25. C.M.A. Brett, *J. Appl. Electrochem.* **20** (1990) 1000.
26. J.H. Wit and H.J.W. Lenderink, *Electrochim. Acta* **41** (1996) 1111.
27. J.W. Lenderink, M. Linden and J.H. Wit and *Electrochim. Acta* **38** (1993) 1989.
28. S.E. Frers, M.M. Stefenel, C. Mayer and T. Chierchie, *J. Appl. Electrochem.* **20** (1990) 996.
29. J.B. Bessone, D.R. Salinas, C. Mayer, M. Ebert and W.J. Lorenz, *Electrochim. Acta* **37** (1992) 2283.
30. J.B. Bessone, C. Mayer, K. Jutner and W.J. Lorenz, *Electrochim. Acta* **28** (1983) 171.
31. J.H. Wit, C. Wijenberg and C. Crevecoeur, *J. Electrochem. Soc.* **126** (1979) 779.
32. G.T. Burstein and R.J. Cinderey, *Corros. Sci.* **32** (1991) 1195.
33. R.J. Cinderey and G.T. Burstein, *Corros. Sci.* **33** (1992) 475, 493, 499.
34. A. Frichet, P. Gimenez and M. Keddam, *Electrochim. Acta* **38** (1993) 1957.
35. K. Jutner, *Electrochim. Acta* **35** (1990) 1501.
36. E. Kalman, B. Varhegyi, I. Felhosi, F.H. Karman and A. Shaban, *J. Electrochem. Soc.* **141** (1994) 3357.